Automatic Surface Matching for the Registration of LIDAR Data and MR Imagery

Ayman F. Habib, Rita W.T. Cheng, Eui-Myoung Kim, Edson A. Mitishita, Richard Frayne, and Janet L. Ronsky

Several photogrammetric and geographic information system applications such as surface matching, object recognition, city modeling, environmental monitoring, and change detection deal with multiple versions of the same surface that have been derived from different sources and/or at different times. Surface registration is a necessary procedure prior to the manipulation of these 3D datasets. This need is also applicable in the field of medical imaging, where imaging modalities such as magnetic resonance imaging (MRI) can provide temporal 3D imagery for monitoring disease progression. This paper will present a general automated surface registration procedure that can establish correspondences between conjugate surface elements. Experimental results using light detection and ranging (LIDAR) and MRI data will verify the feasibility, robustness, and accuracy of this approach.

Keywords: Automatic surface matching, registration, modified iterated Hough transform, iterative closest point.

Manuscript received June 10, 2005; revised Jan. 19, 2006.

This work was supported primarily by the Alberta Ingenuity Fund and National Sciences and Engineering Research Council of Canada, and partially by the Canada Foundation for Innovation.

Ayman F. Habib (phone: + 1 403 220 7105, email: habib@geomatics.ucalgary.ca), Rita W.T. Cheng (email: rwtcheng@ucalgary.ca), and Eui-Myoung Kim (email: emkim@ucalgary.ca) are with Department of Geomatics Engineering, University of Calgary, Canada.

Edson A. Mitishita (email: mitishita@ufpr.br) is with Department of Geomatics, The Federal University of Paraná, Brazil.

Richard Frayne (email: rfrayne@ucalgary.ca) is with Department of Radiology and Clinical Neurosciences, University of Calgary, Canada.

Janet L. Ronsky (email: jlronsky@ucalgary.ca) is with Department of Mechanical and Manufacturing Engineering, University of Calgary, Canada.

I. Introduction

In general, registration is the process of aligning overlapping datasets so that more information and better inference can be derived from combined datasets when compared to those resulting from a single source. Due to differences in the acquisition methodologies, the involved datasets might have different geometric and radiometric characteristics, have unknown correspondences between conjugate elements, and be given relative to different reference frames. Manipulation of these types of data should be preceded by having them co-aligned relative to the same reference frame. In other words, accurate registration is a necessary procedure for a variety of applications such as surface matching, pattern recognition, medical image analysis, environmental monitoring, and change detection. Thus, the registration problem spans several research fields where different methodologies have been developed [1], [2].

With the advances in imaging and computer technologies as well as the higher demand for real-time data processing and analysis, automatic registration has become more widely employed than traditional manual techniques. In general, automatic registration must deal with four issues: 1) registration primitives (for example, points, lines, and regions) that represent the involved datasets; 2) a transformation function that describes the mapping between the reference frames associated with the datasets in question; 3) a similarity measure that mathematically ensures the correspondence of conjugate primitives; and 4) a matching strategy that utilizes the above components to automatically solve the registration problem [2]. The choice of primitives, transformation function, similarity measure, and matching strategy depends on many factors including the nature of the application, data acquisition

modalities, inherent distortions and noise, required accuracy, and available processing and computational resources.

In the fields of photogrammetry and remote sensing, accurate surface matching strategies are crucial for the registration of 3D datasets in several applications such as city modeling, ice sheet monitoring, change detection, and object recognition. The surface data in these applications have been traditionally acquired by ground-based, airborne, or space-borne photogrammetric sensors, where a rich body of positional and semantic information can be collected. Recently, light detection and ranging (LIDAR) systems have been rapidly emerging as a fast, accurate, and cost-effective technology for acquiring 3D data representing physical surfaces. LIDAR systems are directly geo-referenced using high-end global positioning/inertial navigation system (GPS/INS) units and thus can provide direct and accurate 3D coordinates of irregularly distributed object space points at high density. In addition to positional data, modern LIDAR systems can capture intensity images over the mapped objects. As a result of these advances, LIDAR is being more extensively used in mapping and geographic information system applications, and can be combined with photogrammetric systems to provide complementary and complete surface information [3].

The majority of existing surface matching techniques utilize a least squares approach that minimizes the distances between corresponding surface elements to solve for the registration problem [4]-[7]. Some of these techniques require interpolating the available surfaces into a regular grid where elevation differences are minimized at corresponding posts. Surface interpolation can induce errors, especially when dealing with large-scale data over urban areas. Furthermore, minimizing elevation differences is a valid matching procedure only when working with horizontal surfaces [8]. Habib and others [9] proposed a robust surface matching algorithm based on the modified iterated Hough transform (MIHT). In this approach, normal distances, rather than elevation differences, between conjugate surface elements are used to solve the registration problem. Another appealing feature of the MIHT is that it can simultaneously estimate the transformation parameters relating the two surfaces while establishing the correspondence between conjugate surface elements. In addition, this algorithm does not require pre-interpolation of the acquired data. For these reasons, the MIHT offers some key advantages over other surface matching techniques. Hence, the MIHT approach is used in this research after some modification as the surface matching strategy within the registration paradigm. Implementation details regarding the MIHT will be provided later in this paper.

Among the available medical imaging modalities, such as X-ray, ultrasound, and computer tomography, magnetic resonance imaging (MRI) is becoming widely accepted and employed in clinical and medical research. In contrast to other modalities, MRI allows great flexibility in non-invasive acquisition of high resolution and high contrast images. Moreover, it has no known adverse effects on human subjects [10]. The nature of magnetic resonance (MR) is based on the interaction of nuclear spins of hydrogen protons with magnetic fields. An accurately calibrated MR scanner will produce properly scaled 3D data in the form of many cross-sections. Besides the more familiar applications in vascular, stroke, and functional imaging, MR plays an important role in musculoskeletal biomechanics research such as the monitoring of joint health in the presence of degenerative diseases, for example, osteoarthritis (OA). OA is the most common form of arthritis, which mainly affects articular cartilages and bones of weight-bearing joints such as knees and hips [11]. Although there is evidence that biomechanical aggravations, genetic factors, and joint injuries play a role in the development of OA, the exact pathology is not well understood [12]. Therefore, in order to gain more understanding of OA, it is necessary to study the morphology and mechanical properties of cartilages to quantify and analyze joint contact characteristics and assess joint health status over time. For these types of analysis, MRI can provide accurate 3D data of joint structures leading to advances in the understanding of OA and its relationship to joint biomechanics [12], [13]. For these analyses, anatomically corresponding elements in temporal datasets have to be identified and compared. However, within the MR scanner, the subject can be positioned in multiple ways and a different coordinate system is defined for each set of images. As a result, it is quite difficult to capture the same cross-sectional images at corresponding anatomical locations. Moreover, disease progression might lead to anatomical changes; thus a robust registration technique becomes a necessary prerequisite for these applications [14].

As reviewed by Antoine Maintz and Viergever [1], many medical image registration techniques have been developed for different imaging modalities and applications. For the study of articular cartilages and degenerative joint diseases, Stammberger and others [14] introduced an elastic registration technique for cartilage surfaces acquired by MRI to measure local changes in cartilage thickness over time. This method performs the matching by deforming cartilage surfaces, which might pose problems especially if degenerations or changes to these surfaces took place. The authors concluded that local differences in cartilage thickness of approximately 1.0 mm can be reliably detected using MR imagery with a resolution of 0.31 mm × 0.31 mm × 1.5 mm. Despite the availability of many registration techniques, more effective registration methods and data visualization are needed to fully exploit the rich body of quantitative and qualitative information in medical imagery [1].

This paper presents a novel attempt of translating and modifying methods, which were initially developed for

geographic data, for the accurate registration of joint surfaces generated from MRI. Experimental results from both LIDAR and MRI data not only confirm the accuracy of the proposed surface matching and registration algorithm, but also demonstrate its feasibility and robustness in registering medical imagery. The next two sections will provide a detailed description of the proposed algorithm, which will be followed by a detailed discussion of the experimental results from LIDAR and MRI data. Finally, concluding remarks and recommendations for future work will be presented.

II. Registration Paradigm

This section will explain the four components of the proposed registration paradigm: the registration primitives, transformation function, similarity measure, and matching strategy. Moreover, the rationale behind the choice of specific paradigm components will be discussed.

1. Registration Primitives

Primitives are the utilized features for representing and relating the involved datasets in the registration process. For surfaces, the most commonly used registration primitives include points, lines, and areal patches. The chosen primitives depend on the characteristics of the involved data and will directly influence the mechanics of subsequent components of the registration paradigm. The proposed surface matching algorithm works with data in its raw format without the need of any pre-processing procedures (for example, interpolation). Therefore, the two surfaces can be represented by irregularly distributed point clouds that are not necessarily conjugate, that is, there is no point-to-point correspondence, and are given with respect to different reference frames. This choice of primitive is suitable for LIDAR and MRI data, where features of interest (for example, terrain, buildings, or bones) are represented by a cloud of randomly distributed points that are spatially defined by their 3D coordinates. Since no point-to-point correspondence can be assumed, points in one of the surfaces are further processed to form triangular patches, similar to a triangulated irregular network. It should be noted that since the two datasets are typically acquired by the same sensor, they would exhibit the same data characteristics (for example, point density), thus the algorithm and results would not be affected by the choice of surface presentation for each dataset (that is, which surface is represented by points and which is by patches). In other words, deviations between a set of results and those obtained after swapping the representation schemes would not exceed the noise level in the implemented data. Figure 1 depicts a simple example of the registration primitives used in the proposed surface matching algorithm: points for one surface (S_1) and patches for the other surface (S_2).

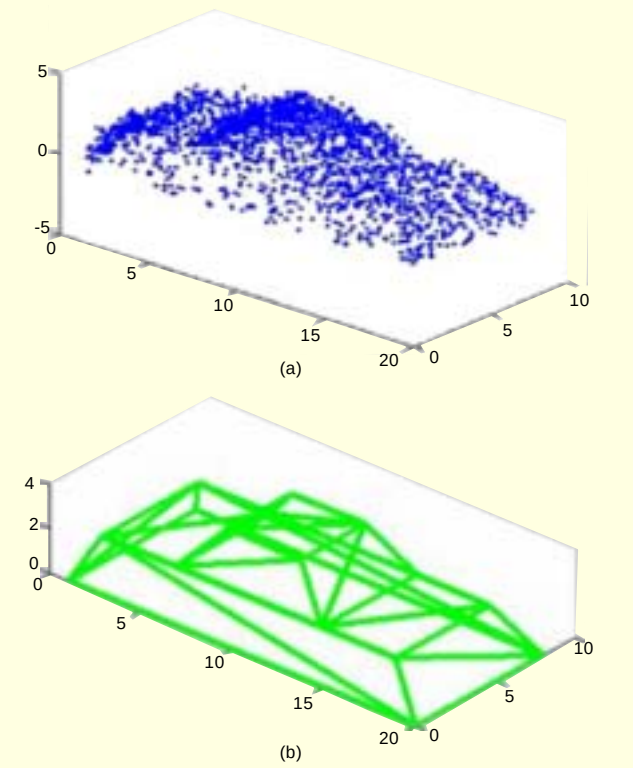

Fig. 1. Registration primitives for the proposed surface matching algorithm: (a) points for S_1 and (b) triangular patches for S_2.

2. Transformation Function

In general, the involved datasets in a registration problem might be given relative to different reference frames. The transformation function describes the mathematical relationship or mapping function between the reference frames associated with the two surfaces. More specifically, the transformation function maps the primitives from S_1 onto the corresponding primitives in S_2. The chosen transformation function for the proposed surface registration is 3D similarity, which includes seven parameters: three translations along the coordinate axes (X_T, Y_T, Z_T), three rotations (ω, φ, κ), and a scale factor (S); refer to (1). These seven parameters relating S_1 and S_2 are assumed to be unknowns and are solved for as part of the registration problem.

$$\begin{bmatrix} X' \\ Y' \\ Z' \end{bmatrix} = \begin{bmatrix} X_T \\ Y_T \\ Z_T \end{bmatrix} + S \times R(\omega, \varphi, \kappa) \begin{bmatrix} X \\ Y \\ Z \end{bmatrix}, \quad (1)$$

where, X, Y, Z are the coordinates of a point on the first surface, X', Y', Z' are coordinates of the transformed point with respect

to the second surface reference frame, and R is a 3 by 3 matrix that describes the rotational relationship between the involved reference frames.

This transformation is a rigid-body and global transformation, which means that one set of transformation parameters is used to relate the two surfaces. Moreover, such a transformation assumes the absence of any deformations between the two surfaces that cannot be modeled by a rigid-body transformation. However, the presence of these deformations can be inferred by evaluating the quality of fit between registered surfaces.

3. Similarity Measure

The similarity measure mathematically describes the coincidence of conjugate registration primitives after performing the appropriate transformation function. The formulation of the similarity measure depends on the choice of primitives as well as the utilized transformation function. Since points and patches are used as the registration primitives to describe the involved surfaces (S_1 and S_2, respectively), the similarity measure should constrain a transformed point, q, from S_1 to be coplanar with its conjugate patch from S_2 as defined by its vertices p_a, p_b, and p_c, as shown in Fig. 2. In other words, if point q is assumed to belong to a specific surface patch, the normal distance (d) between q', which is obtained by applying the appropriate 3D similarity transformation on q, and the corresponding patch in S_2 should be zero. This condition is known as the coplanarity condition and is mathematically described by (2), which states that the volume enclosed by a point and the corresponding patch is zero. If more than seven conjugate point-patch pairs are identified, the transformation parameters, which are implicitly present in the first row of (2), can be solved for by satisfying the coplanarity constraints through a least squares adjustment procedure. It should be noted that this similarity measure reduces the normal distances between corresponding surface elements rather than reducing

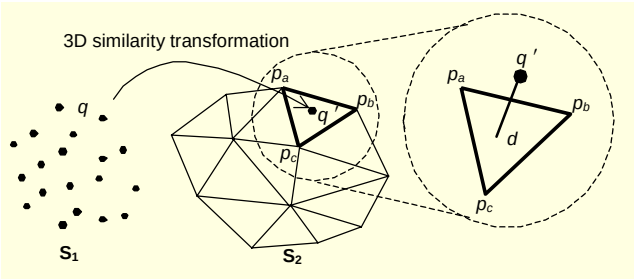

Fig. 2. Coplanarity condition describes the correspondence between a point in S_1 and a patch in S_2 after performing a 3D similarity transformation.

elevation differences. Thus, it is valid for surfaces with any orientation, which could be the case for large-scale LIDAR data and MR imagery. Moreover, the parameters of the transformation function can be accurately solved for only if surface patches with varying orientation are available. For example, horizontal surfaces will only allow for estimating the shift component in the Z direction, Z_T, as well as the rotation angles ω and φ.

$$\begin{vmatrix} X_{q'} & Y_{q'} & Z_{q'} & 1 \\ X_{p_a} & Y_{p_a} & Z_{p_a} & 1 \\ X_{p_b} & Y_{p_b} & Z_{p_b} & 1 \\ X_{p_c} & Y_{p_c} & Z_{p_c} & 1 \end{vmatrix} = 0 \qquad (2)$$

4. Matching Strategy

The matching strategy is an optimization procedure that utilizes the primitives, transformation function, and similarity measure to automate the registration procedure by establishing the correspondences between conjugate surface elements as well as the parameters of the transformation function. As previously mentioned, if seven or more conjugate point-patch pairs are identified, the transformation parameters can be solved for using the coplanarity constraints as in (2). However, since the correspondences between the two surfaces are typically unknown, conjugate point-patch pairs have to be identified either manually or automatically. Manual identification of conjugate point-patch pairs is difficult if not impossible, especially when considering the volume of involved datasets. To overcome this issue, a modified iterated Hough transform (MIHT) is proposed as the matching strategy based on a voting scheme to simultaneously establish the correspondences between surface elements and solve for the transformation parameters.

The role of the voting scheme within the MIHT is to identify the most probable solution for the transformation parameters by considering all possible matches between points in S_1 and patches in S_2. To illustrate the voting concept, one can consider any seven points in S_1 and any seven patches in S_2. If each point is assumed to match one of the patches, the relationship between these pairs can be described by a set of transformation parameters that results from the solution to the seven coplanarity constraints. Another seven point-patch pairs can be chosen to derive another set of parameters. If this process is repeated for all possible matches while keeping track of the derived solutions, correct matches will result in the same solution for the parameters. Therefore, the voting scheme will simultaneously establish the correspondences between conjugate primitives as well as derive an estimate of the transformation parameters. To keep track of the resulting solutions from the hypothesized matches, a seven-dimensional accumulator array is required, where the frequency of each solution vector in this array is recorded. The correct solution

will have the highest votes and will manifest itself as a peak in the accumulator array. However, the use of a seven-dimensional accumulator array involving a large number of primitives, while keeping track of possible primitive pairings, is computationally intensive and will eventually lead to a combinatorial explosion. To overcome this problem, the MIHT approach solves for the parameters sequentially and iteratively by implementing a one-dimensional accumulator array while considering one parameter and one hypothesized matching pair at a time. In other words, the MIHT procedure replaces the seven-dimensional accumulator array with seven one-dimensional accumulator arrays. Moreover, instead of considering seven matching pairs, the MIHT works with one single matching pair at a time. The following section describes the proposed automated surface matching and registration methodology that incorporates the above mentioned registration paradigm components.

III. Automated Surface Matching and Registration Methodology

The proposed matching and registration methodology begins by setting up initial approximations for the unknown parameters of the transformation function. Subsequently, one of the parameters, for example X_T, is estimated through a one dimensional accumulator array that keeps track of the derived solutions from all possible hypothesized point-patch pairs between S_1 and S_2, while considering the other parameters to be correct. In other words, the coplanarity constraint resulting from a hypothesized matching pair will be used to solve for only one parameter. The accumulator array is a discrete tessellation of the expected solution range of the parameter in question. The cell size and range of the accumulator array depend on the quality of the approximate value for the non-considered parameters. Rough approximations should be compensated for by a large range and cell size. The peak of the populated accumulator array will indicate the most probable solution of the parameter in question, as shown in Fig. 3. The initial approximation for that parameter is updated with this peak value. This estimation process is then repeated sequentially for each of the remaining parameters. Furthermore, the procedure for estimating the seven parameters is iterated while decreasing the cell size of the accumulator array as well as its extent/range to reflect the improvement in the derived estimates of the transformation parameters. In this manner, the unknown parameters are iteratively solved for in a coarse-to-fine strategy. The estimated parameters will converge to the most probable solution. In other words, when convergence is achieved, the estimated parameters will not significantly change between two successive iterations.

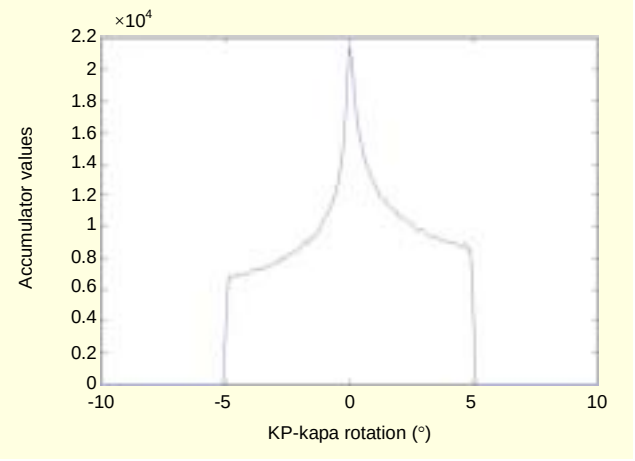

Fig. 3. An accumulator array with the peak indicating the most probable solution for the parameter in question.

Unfortunately, due to inherent noise in the data acquisition and possible errors introduced by data processing (for example, feature digitization in MRI and measurement units in LIDAR), the algorithm might not always converge. The non-convergence probability will be higher with the increase in the density of the surface points reaching a critical stage when the point density is almost equivalent to the level of the noise in the acquired points. This problem should be expected when dealing with high resolution LIDAR and MRI data. To overcome this limitation, MIHT is complemented by the iterative closest point (ICP) procedure [15]. ICP is utilized to iteratively establish the correspondence between the surface elements and accurately solve for the seven transformation parameters. However, the ICP capability depends on the quality of the initial approximations. Having rough approximations will most probably lead to the ICP converging to a local minimum. In this regard, the combination of the MIHT and ICP strategies is optimal since the MIHT procedure will ensure the availability of good approximations, which could be further refined through the ICP approach. Figure 4 shows a comparison of the convergence of the parameter φ based on only the MIHT approach and the combined MIHT/ICP approach. It is clear that ICP complements MIHT and refines the convergence of the parameter.

As the name suggests, using approximate parameters, the ICP finds the closest patch in S_2 for each point in S_1 and considers them as a matching pair. Using the resulting matches for the involved points in S_1, the ICP procedure estimates an updated solution vector through a least squares adjustment. Estimated parameters are then used to derive updated matching pairs, which are used again to update the solution vector. This procedure is repeated until convergence where the estimated

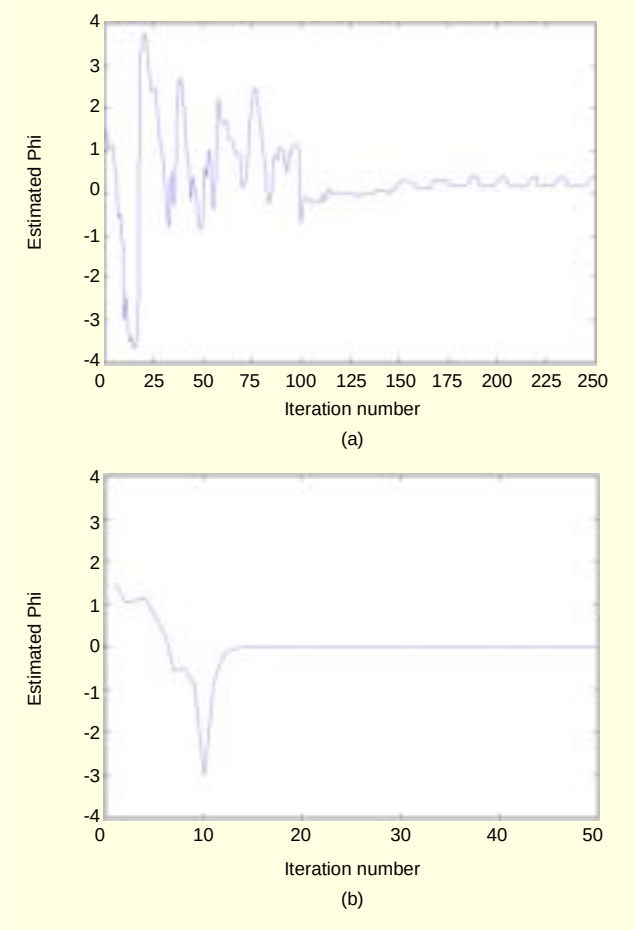

Fig. 4. Convergence for the angle φ with (a) the MIHT approach and (b) the combined MIHT/ICP approach.

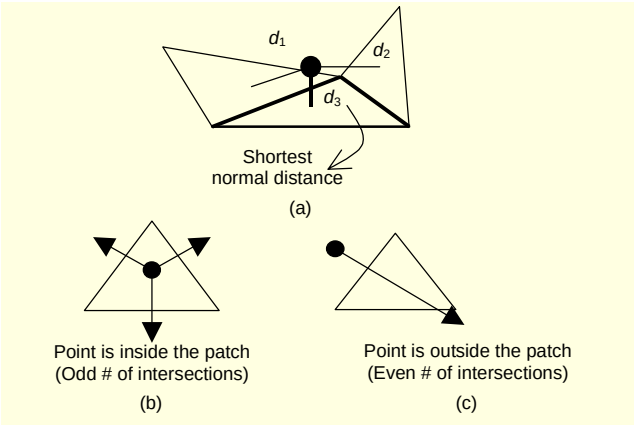

Fig. 5. Matching criterion 1: (a) shortest normal distance. Matching criterion 2: (b) projected point is inside and (c) outside the patch.

parameters do not significantly change between two successive iterations. In our implementation of the ICP, as shown in Fig. 5, a point and a patch are considered as a matching pair if the following criteria are satisfied:

Shortest normal distance: A point matches a patch when the normal distance is less than a certain threshold and is also the shortest distance compared to the other patches. The threshold value depends on the amount of noise inherent in the involved data.

Projected point is inside the patch: A point matches a patch if its projection onto the patch is inside the polygon defined by its vertices. The decision of whether the projected point is inside or outside the patch is determined by the number of intersections a shooting ray from that point makes with the edges of the patch.

Unmatched points within the ICP procedure can be classified as changes or blunders. In this regard, the combined MIHT/ICP approach is highly robust to changes and outliers in the involved datasets due to the fact that only matches will be considered in the estimation of the transformation parameters. The quality of fit between the registered surfaces can be measured by the variance component resulting from the least squares adjustment procedure. A smaller variance component indicates a better fit. In addition, the quality of fit can be evaluated by the root mean squares (RMS) of the normal distances between the matched point-patch pairs. The RMS of the normal distances provides a meaningful and direct measure of the quality of the registration outcome. In summary, the proposed automated surface matching and registration procedure can be described by the flow chart in Fig. 6.

As a concluding remark, the proposed algorithm can be applied to match small as well as extended areas. The size of the area will only influence the execution time of the algorithm. The extent of the involved area of the dataset for matching

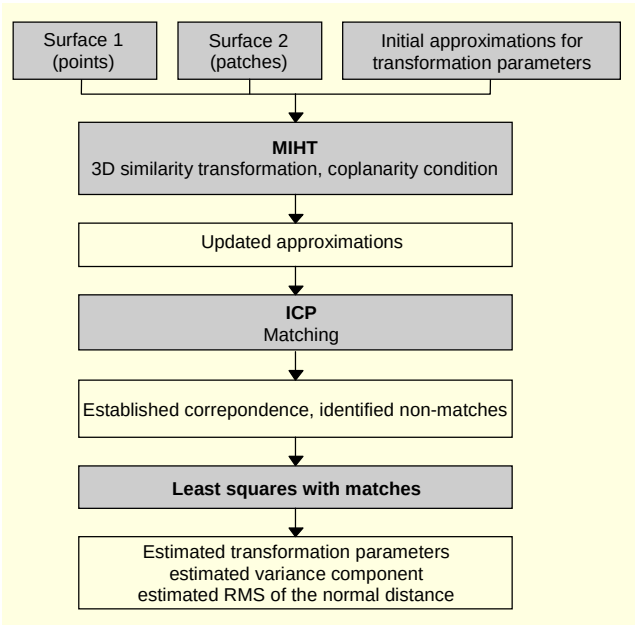

Fig. 6. Automated surface matching and registration algorithm.

depends on the underlying objectives of the surface matching procedure. For example, if surface matching is applied for quality control of a LIDAR system, one can match the entire region in the overlap area between adjacent strips. Alternatively, one can work with a set of smaller and well distributed regions in the overlap area. For change detection applications, on the other hand, the proposed algorithm can be applied to larger areas. For all these applications, it is crucial to have sufficient surface geometry (that is, variations in the surface topography) for accurate estimations of the transformation parameters.

IV. Experimental Results

To verify the feasibility of the proposed matching and registration methodology, several experiments using LIDAR and MRI data are conducted. The following sub-sections describe the involved data in each experiment, the necessary pre-processing procedures for surface generation, and the respective results/discussions.

1. LIDAR

In this experiment, the performance of the proposed registration algorithm is checked by the automated matching of two adjacent and overlapping LIDAR strips. The utilized LIDAR data covers an urban area in Brazil and is given with respect to the World Geodetic System 1984 (WGS84) reference frame. This dataset was captured by an OPTECH ALTM 2050 airborne laser scanner from an average flying height of 975 m. The point density for these strips is approximately 2.24 points/m^2, with S_2 and S_1 comprised of 22,799 and 44,156 points, respectively. According to the flight and sensor specifications, this data is expected to have a horizontal accuracy of 0.5 m and a vertical accuracy of 0.15 m.

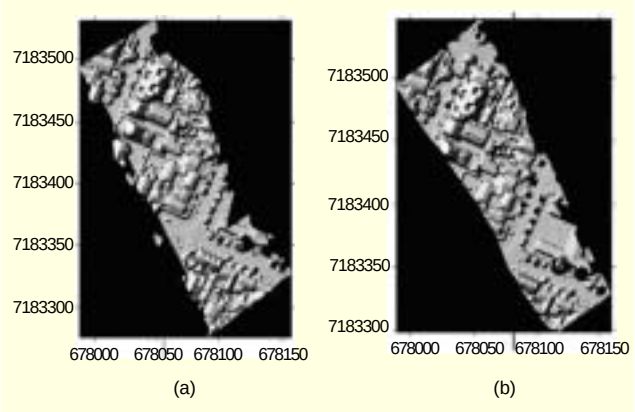

Fig. 7. Overlapping LIDAR range images over an urban area: (a) S_1 and (b) S_2.

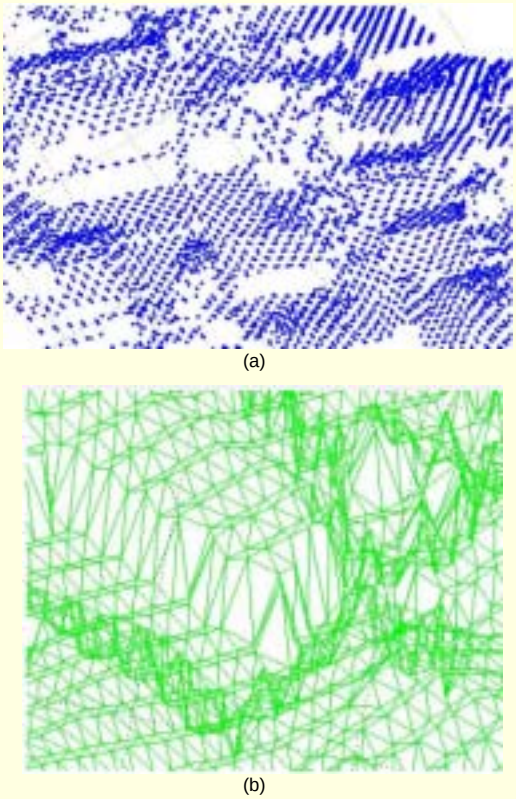

Fig. 8. Sections of (a) the first LIDAR surface represented by 44,156 points and (b) the second surface modeled by 45,520 triangular patches.

Figure 7 shows range images of the overlap area between S_1 and S_2, which mainly covers buildings, vegetation (for example, trees), roads, and other man-made structures. The 22,799 points of S_2 were used to generate 45,520 triangular patches based on Delaunay triangulation.

Figure 8 displays a closer look at corresponding windows in these strips. It shows that due to the nature of LIDAR data acquisition, only a small number of points were captured on the vertical facets of buildings, the blank areas in Fig. 8(a).

Since the LIDAR strips are given relative to the same reference frame, WGS84, the transformation parameters (X_T, Y_T, Z_T, ω, φ, κ, S) relating these strips should assume the values *0* m, *0* m, *0* m, *0°*, *0°*, *0°*, and *1*, respectively. However, such values will only be valid if there are no biases in the data acquisition system. For the MIHT procedure, the cell sizes for the accumulator arrays ranged from 1.0 to 0.2 m for the shifts, 0.10 to 0.01 for the scale factor, and 1.0° to 0.5° for the rotations. A distance threshold of 0.5 m was used for the first matching criterion. Due to the large numbers of points and patches, the algorithm took approximately 1 day to complete with a 3.0 GHz computer. Table 1 shows the results from the automated registration of S_1 and S_2 using the proposed surface

Table 1. Initial approximations, expected parameters, estimated transformation parameters, and registration results of the LIDAR data.

	X_T (m)	Y_T (m)	Z_T (m)	S	ω (°)	φ (°)	κ (°)
Initial approximations	3.000	-3.000	3.000	0.900	-3.000	3.000	-3.000
Expected parameters	0.000	0.000	0.000	1.000	0.000	0.000	0.000
Estimated parameters (± standard deviation)	-0.660 (1.26e-3)	-0.367 (1.55e-3)	0.007 (2.44e-3)	1.001 (2.20e-5)	-0.017 (6.40e-5)	0.002 (1.14e-4)	0.003 (1.80e-5)
Estimated variance component	0.122						
RMS of the normal distances	0.142 m						

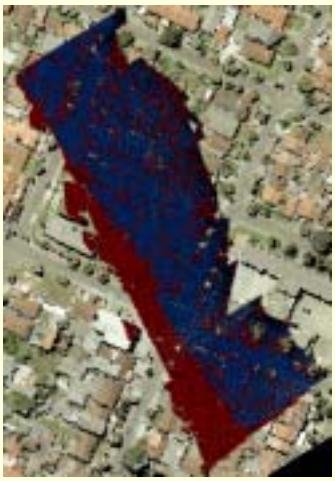

Fig. 9. Matched (blue) and unmatched-points (red) of the first surface displayed on an ortho-photo of the target area.

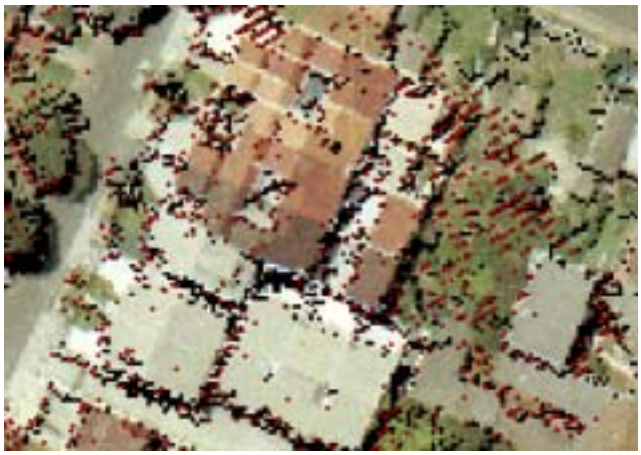

Fig. 10. Unmatched points (red) are mainly located along building boundaries and around areas with vegetation.

matching algorithm. As shown in Table 1, the initial approximations are chosen to be significantly different from the expected values to test the performance of the proposed strategy. The RMS of the normal distances between the matched point-patch pairs is found to be 0.142 m, which indicates an accurate registration, considering the horizontal and vertical accuracy of the involved data. It is also important to note that poor initial approximations still lead to accurate estimations of the transformation parameters. The deviations of the estimated transformation parameters from the expected values indicate that some biases do exist between the two strips. The larger deviations for X_T and Y_T might result from bore-sighting biases between the GPS/INS unit and the laser system. However, these biases are still within the noise level in the data. In summary, the reported results in Table 1 indicate that there are no significant biases between the LIDAR strips, which cannot be modeled by a rigid body transformation.

A qualitative analysis of the results can further verify the accuracy of the registration. In Fig. 9, the matched (blue) and unmatched (red) points in S_1 are overlaid on top of an ortho-photo of the target area. The group of unmatched points on the left edge of the target area is due to a small section of a non-overlapping portion covering S_1. Figure 10 shows a closer look at a portion of unmatched points within the overlap area. As can be seen in this figure, the unmatched points are mainly located along building boundaries and around areas with vegetation. Such an observation is justified by the fact that physical surface representation using planar patches is not valid at building boundaries (where the patches are formed by vertices on the ground and building tops) and in vegetation areas (where LIDAR rays can penetrate through to reach lower levels of vegetation or the ground); refer to Fig. 8(b).

To further validate the accuracy of the surface matching and registration algorithm, the estimated transformation parameters are compared to those obtained using manually extracted and identified conjugate linear features. Registration by utilizing linear features can provide accurate results as they can be reliably and accurately extracted from LIDAR data [16].

In a parallel study to this work, 164 conjugate lines were extracted from the same LIDAR strips. The extraction of the linear features starts with the identification of planar patches in each strip. Afterwards, neighboring patches with different orientation are intersected to produce the linear features. These features are then used in a line-based absolute orientation

Table 2. Transformation parameters derived based on linear features and from surface matching for the LIDAR data.

Registration method	X_T (m)	Y_T (m)	Z_T (m)	S	ω (°)	φ (°)	κ (°)
Linear features and absolute orientation (± standard deviation)	-0.418 (2.98e-2)	-0.209 (2.79e-2)	-0.019 (7.87e-2)	1.000 (2.30e-5)	-0.010 (2.29e-2)	0.017 (3.78e-2)	0.003 (1.30e-3)
Surface matching (± standard deviation)	-0.660 (1.26e-3)	-0.367 (1.55e-3)	0.007 (2.44e-3)	1.001 (2.20e-5)	-0.017 (6.40e-5)	0.002 (1.14e-4)	0.003 (1.80e-5)

procedure to solve for the transformation parameters between the strips [16]. The estimated transformation parameters from the line-based absolute orientation are summarized in Table 2, along with the results from the surface matching algorithm. It can be seen that the transformation parameters from both approaches are similar, especially when considering the noise level in the LIDAR data and the preprocessing procedure for the derivation of the linear features. Thus, this comparison has validated the accuracy of the proposed surface matching and registration algorithm. It should be noted that although the surface registration using linear features can produce accurate results, the presented procedure in this paper is more advantageous since it directly works with the raw LIDAR point clouds with minimal pre-processing. Furthermore, for areas with a limited number of linear features, the presented approach will be more appropriate.

The above experiment confirms the feasibility and accuracy of the proposed surface matching algorithm for registering remotely sensed data. It suggests the presence of some biases between the LIDAR strips. However these biases are within the noise level in the data and therefore their presence could not be verified. The next section will further demonstrate the feasibility of the same algorithm for registering anatomical surfaces based on MRI.

2. MRI

For this experiment, temporal MR imagery of a knee joint was acquired with a balanced steady-state free precession sequence on a 3-Telsa General Electric MR unit located at the Seaman Family MR Research Centre, Foothills Medical Centre, Calgary. The unit is shown in Fig. 11. Ethics approval was obtained from the Conjoint Health Research Ethics Board, University of Calgary, for performing health research on human subjects. Written informed consent was also obtained from each subject prior to imaging. The subject's lower limb was positioned by a custom-designed loading apparatus inside the MR scanner gantry [17]. The first set of images of the knee joint was acquired with the lower limb flexed at a 30° angle, as shown in Fig. 12(a). On the other hand, the second dataset was

Fig. 11. 3-Telsa GE MR unit used for MR imagery acquisition.

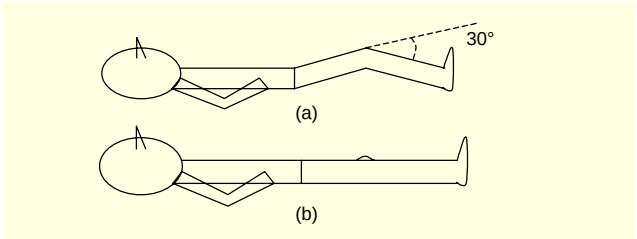

Fig. 12. Subject positioned at (a) a 30° knee flexion angle for the first dataset, and at (b) 0° (full extension) for the second dataset.

captured with the limb at full extension, as shown in Fig. 12(b). Both datasets contain 36 sagittal images with a 0.625 mm in-plane resolution (that is, image pixel size) and 3.000 mm across-slice resolution (slice thickness). Thus, each image voxel has a size of 0.625 mm × 0.625 mm × 3.000 mm. Figure 13 illustrates a sample image slice from each dataset.

To generate 3D surfaces from raw MRI data, points are manually digitized along the bone-cartilage interface of the femur (thigh bone) for each image slice using SliceOmatic software, Tomovision, Canada. The red points in Fig. 13 illustrate the digitized points along the femur for those image slices. These points form contours of the femur surface. The

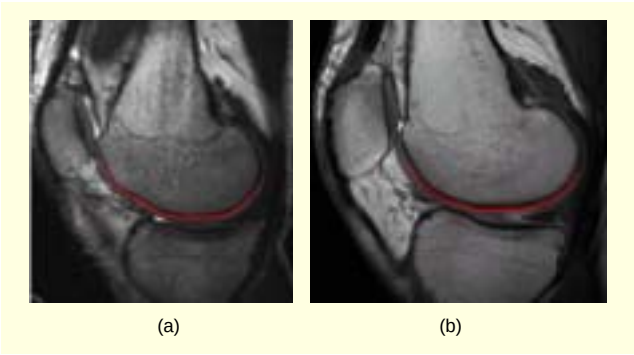

(a) (b)

Fig. 13. MR image slices from (a) the first dataset with a 30° knee flexion and (b) the second dataset with the lower limb at full extension.

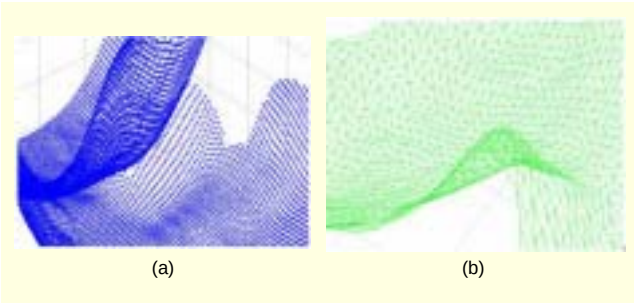

(a) (b)

Fig. 14. Sections of (a) the first MRI surface represented by 15,085 points and of (b) the second surface (reference surface) modeled by 6,789 triangular patches.

bone surface is assumed to remain rigid at different flexion angles. It is important to note that even if some local changes occur along the bone surface over time, these changes will be isolated by the proposed algorithm as non-matches and will not be included in the least squares solution of the transformation parameters.

Due to the lower resolution in the across-slice direction, the points are densified by a thin plate spline (TPS) algorithm [18]. The resampled points in one of the datasets are then used to generate triangular patches using Delaunay triangulation to model the second surface S_2. Sections of the involved surfaces in this experiment after performing the above pre-processing procedures are shown in Fig. 14, with S_1 represented by 15,085 points (TPS resampling rate: 0.5 mm) and S_2 modeled by 6,789 triangular patches (TPS resampling rate: 1.0 mm).

For the surface matching algorithm, the cell sizes of the MIHT procedure ranged from 0.8 mm to 0.5 mm for the shifts, 0.10 to 0.01 for the scale factor, and 1.0° to 0.5° for the rotations. A 0.4 mm distance threshold was used for classifying matches. The algorithm took 2 hr 20 min to process using a 3.0 GHz processor. Table 3 summarizes the results from the registration of the two MR surfaces using the proposed surface matching algorithm. Due to the different knee flexion angles and subject re-positioning between the dataset acquisitions, significant translations and rotations are expected. The expected true values for these parameters are unknown since no control markers were used during data acquisition. However, the scale between these datasets is expected to be 1.0 since MRI captures the true dimensions of scanned objects. The estimated RMS of the normal distances between matched point-patch pairs turned out to be 0.201 mm. Such a value indicates a high level of accuracy considering the resolution of the involved MR images.

A visual display of the matched and unmatched points is shown in Fig. 15. The unmatched points (red) around the edges are believed to result from possible errors introduced during the digitization process as well as discrepancies between the surfaces caused by the different re-sampling resolutions used in TPS. Since only the bone cartilage interface has been used for the registration, it is important to evaluate whether this is sufficient to produce a good alignment of the whole femur. Such an evaluation is achieved by simultaneously displaying corresponding image slices after applying the estimated transformation parameters, as shown in Fig. 16. The transformed images were then re-sampled so that they fell onto the same planes as the reference image slices. A closer look at the mosaics in Fig. 16 reveals that even though a small portion of the femur is used for the registration, corresponding features from other areas are also well-aligned.

Table 3. Initial approximations, expected true parameters, estimated transformation parameters, and registration results of the MRI data.

	X_T (mm)	Y_T (mm)	Z_T (mm)	S	ω (°)	φ (°)	κ (°)
Initial approximations	0.000	0.000	0.000	0.900	0.000	0.000	0.000
Expected parameters	N/A	N/A	N/A	1.000	N/A	N/A	N/A
Estimated parameters (± standard deviation)	0.770 (1.37e-2)	-0.518 (7.33e-3)	1.049 (4.85e-3)	0.997 (2.91e-4)	-2.088 (1.90e-4)	-9.301 (4.99e-4)	-2.973 (1.76e-4)
Estimated variance component	0.044						
RMS of the normal distances	0.201 mm						

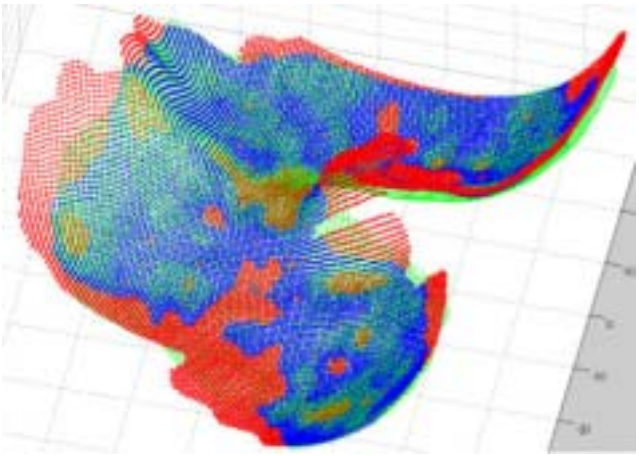

Fig. 15. Co-registered MRI surfaces with the green mesh representing the reference surface (S_2), blue points representing the matched points, and red points representing the non-matches in the first surface (S_1).

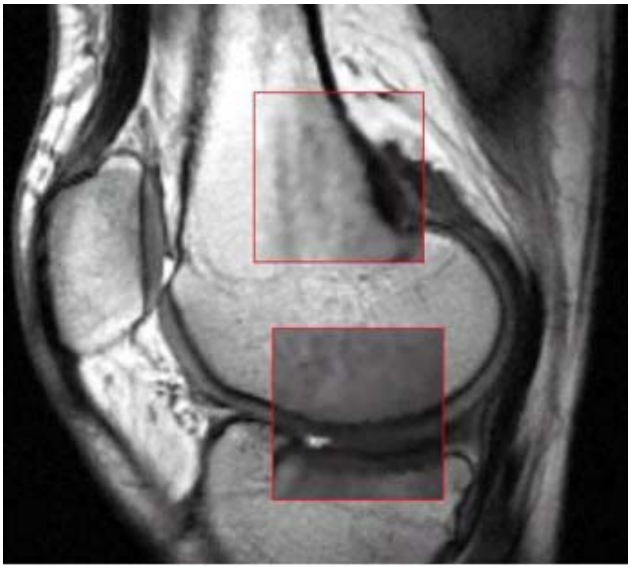

Fig. 16. Mosaics showing a good match between the reference image from the first dataset (background) and its corresponding image from the second dataset (foreground/small windows).

V. Conclusions and Future Works

For both photogrammetric and medical imaging applications dealing with data acquired by different modalities and/or at different times, accurate surface registration strategies are essential. This paper introduced a robust and automatic surface matching and registration algorithm that can establish correspondences between conjugate surface elements while accurately estimating the transformation parameters. The proposed approach addressed the appropriate primitives, transformation function, similarity measure, and matching strategy for automated matching and registration of 3D data. The algorithm is general enough that it can be applied in the registration of LIDAR and MR surfaces. The modified iterated Hough transform (MIHT) is used as the matching strategy that evaluates the correspondences between conjugate elements while filtering out discrepancies using a voting scheme. To cope with the high point density in the acquired LIDAR and MR imagery, the MIHT is coupled with the iterative closest point (ICP) procedure to assure the convergence of the automated registration process. Experimental results have shown the capability of the proposed methodology in accurately and robustly aligning LIDAR and MR 3D datasets. The robustness stems from the fact that discrepancies are filtered out prior to the least squares solution of the unknown parameters.

For future work, the authors propose to improve the overall system's efficiency through the application of the introduced methodology in a coarse-to-fine strategy. This can be done by first using a generalized version of the surfaces to achieve approximate values for the transformation parameters. These estimates can then be improved by restarting the process with less-generalized versions of the surfaces. This process would be repeated while increasing the resolution and reducing the MIHT iterations thus reducing the overall execution time. Another future direction of this research is to apply the surface matching algorithm to a wider range of applications. In fact, the algorithm was applied to successfully register data acquired by a close-range laser system, and this application will be reported in a future publication.

In this research, the quality of the automated registration of LIDAR strips has been checked by a relative comparison with the registration results from manually identified linear features. Also, the presence of biases was identified in the LIDAR data as deviations were found between the estimated transformation parameters and the optimum values (zero shifts and rotations). The future extension of this application is to investigate and justify for the identified biases, and perform bias compensation.

For the MRI experiment, future research will focus on validating the registration accuracy of MRI data. Since a gold standard is typically unavailable for *in vivo* human studies, the validation will be performed by using a cadaver joint (porcine). Linear control markers (for example, glass tubes) will be implanted into the joint tissues and used as the registration primitives for deriving the transformation parameters to validate the ones obtained from the proposed surface registration. In addition, factors that might affect the registration accuracy, such as image resolution, digitization, and surface generation, will be identified and their influence will be analyzed. Successfully registered MR data will be used to study joint biomechanics and detect local changes over time

resulting from disease progression. Such a study will increase our understanding of osteoarthritis and will lead to more effective approaches for the diagnosis, evaluation, and treatment of patients.

Acknowledgement

We would like to recognize the Technology Institute for Development – LACTEC – UFPR for supplying the LIDAR data. We would also like to thank M. Ghanma (PhD Student, University of Calgary) for his help with LIDAR data processing, A. Pullivelli (MSc student, University of Calgary) for his editorial review, and K. Connolly (MSc student, University of Calgary) for her collaborative effort in MR data acquisition.

References

[1] J.B. Antoine Maintz and M.A. Viergever, "A Survey of Medical Image Registration," *Medical Image Analysis*, vol. 2, no. 1, Mar. 1998, pp. 1-36.

[2] L.G. Brown, "A Survey of Image Registration Techniques," *ACM Computing Surveys*, vol. 24, no. 4, Dec. 1992, pp. 325-376.

[3] A. Habib, M. Ghanma, and E. Mitishita, "Co-registration of Photogrammetric and LIDAR Data: Methodology and Case Study," *Brazilian Journal of Cartography*, vol. 56, no. 1, July 2004, pp. 1-13.

[4] H. Ebner and T. Ohlhof, "Utilization of Ground Control Points for Image Orientation without Point Identification in Image Space," *Int'l Archives of Photogrammetry and Remote Sensing*, vol. 30, no. 3/1, Aug. 1994, pp. 206-211.

[5] Y. Postolov, A. Krupnik, and K. McIntosh, "Registration of Airborne Laser Data to Surfaces Generated by Photogrammetric Means," *Int'l Archives of Photogrammetry and Remote Sensing*, vol. 32(3W14), Nov. 1999, pp. 95-99.

[6] Z. Xu and Z. Li, "Least Median of Squares Matching for Automated Detection of Surface Deformations," *Int'l Archives of Photogrammetry and Remote Sensing*, vol. 33, no. B3/2, 2000, pp. 1000-1007.

[7] A. Gruen and D. Akca, "Least Squares 3D Surface Matching," *Proc. ASPRS 2005 Annual Conference "Geospatial Goes Global: From Your Neighbourhood to the Whole Planet"*, 2005.

[8] A. Habib and T. Schenk, "A New Approach for Matching Surfaces from Laser Scanners and Optical Scanners," *Int'l Archives of Photogrammetry and Remote Sensing*, 32(3W14), Nov. 1999, pp. 55-61.

[9] A. Habib, Y. Lee, and M. Morgan, "Surface Matching and Change Detection Using a Modified Hough Transformation for Robust Parameter Estimation," *Photogrammetric Record*, vol. 17, no. 98, Oct. 2001, pp. 303-315.

[10] D. Nishimura, *Principles of Magnetic Resonance Imaging*, Department of Electrical Engineering, Stanford University, 1996.

[11] Arthritis Society, Osteoarthritis, Retrieved on April 29, 2005, from http://www.arthritis.ca/types%20of%20arthritis/osteoarthritis/default.asp?s=1, 2004.

[12] F. Eckstein, M. Reiser, K.-H. Englmeier, and R. Putz, "In Vivo Morphometry and Functional Analysis of Human Articular Cartilage with Quantitative Magnetic Resonance Imaging – from Image to Data, from Data to Theory," *Anatomy and Embryology*, vol. 203, no. 3, Feb. 2001, pp. 147-173.

[13] E. Calvo, I. Palacios, E. Delgado, J. Ruiz-Cabello, P. Hernandez, O. Sanchez-Pernaute, et al., "High-Resolution MRI Detects Cartilage Swelling at the Early Stages of Experimental Osteoarthritis," *Osteoarthritis and Cartilage*, vol. 9, no. 5, July 2001, pp. 463-472.

[14] T. Stammberger, J. Hohe, K.-H. Englmeier, M. Reiser, and, F. Eckstein, "Elastic Registration of 3D Cartilage Surfaces from MR Image Data for Detecting Local Changes in Cartilage Thickness," *Magnetic Resonance in Medicine*, vol. 44, no. 4, Oct. 2000, pp. 592-601.

[15] P.J. Besl and N.D. McKay, "A Method for Registration of 3-D Shapes," *IEEE Transactions on Pattern Analysis and Machine Intelligence*, vol. 14, no. 2, Feb. 1992, pp. 239-256.

[16] A. Habib, M. Ghanma, M. Morgan, and R. Al-Ruzouq, "Photogrammetric and LIDAR Data Registration Using Linear Features," *Journal of Photogrammetric Engineering and Remote Sensing*, vol. 71, no. 6, June 2005, pp. 699-707.

[17] J. Ronsky, *In-vivo Patellofemoral Joint Contact*, doctoral dissertation, University of Calgary, Calgary, Alberta, Canada, 1994.

[18] S.K. Boyd, J.L. Ronsky, D.D. Lichti, D. Salkauskas, and M.A. Chapman, "Joint Surface Modeling with Thin-Plate Splines," *Journal of Biomechanical Engineering*, vol. 121, no. 5, Oct. 1999, pp. 525-532.

Ayman F. Habib received the MSc degree in civil engineering from Cairo University, Egypt, and the MSc and PhD degrees in photogrammetry from Ohio State University, USA. Currently, he is an Associate Professor at the Department of Geomatics Engineering, University of Calgary, Canada. His research interests span the fields of terrestrial and aerial mobile mapping systems, modeling the perspective geometry of imaging scanners, automatic matching and change detection, incorporation of linear features in various orientation procedures, object recognition in imagery, and integration of photogrammetric data with other sensors/datasets.

Rita W.T. Cheng received the BSc degree in geomatics engineering from the University of Calgary, Canada, in 2003. She is currently an MSc student in the Biomedical Engineering program, Department of Geomatics Engineering, at the University of Calgary, Canada, and expects to graduate in June 2006. Her main research interest is in image registration and surface matching of 3D magnetic resonance imagery for the studies of osteoarthritis. She also applies registration techniques for photogrammetric and remote sensing applications with 3D data such as LIDAR.

Eui-Myoung Kim received the MSc degree in urban engineering from Gyeongsang National University, Jinju, Korea, in 1996, and the PhD in civil engineering from Yonsei University, Seoul, Korea, in 2000. From 2000 to 2002, he was the Senior Researcher in Korea Institute of Construction Technology, Goyang, Korea. He worked as a Post-Doctoral Fellow at the University Calgary, Canada from 2003 to 2005. Currently, he is a Deputy General Manager of Korea geoSpatial Information and Communication Co., Seoul, Korea. His research interests include sensor modeling of satellite imagery, DEM generation from high-resolution satellite imagery, and three-dimensional GIS.

Edson A. Mitishita received the BS degree in cartography engineering, the Masters degree in geodetic sciences, and the PhD degree in forest engineering from the Federal University of Paraná, Brazil. He worked as a Post-Doctoral Fellow at the Department of Geomatics Engineering, University of Calgary, Canada, in 2005. Currently, he is a Professor at the Sciences of the Earth Sector, Department of Geomatics, the Federal University of Paraná, Brazil. His scientific research topics relate to digital photogrammetry, remote sensing, and image and laser scanner data mapping development.

Richard Frayne holds the BSc degree from the University of Waterloo, Canada, 1989, and the PhD degree from the University of Western Ontario, Canada, 1994. He is currently an Associate Professor in the Departments of Radiology and Clinical Neuroscience, and a member of the Hotchkiss Brain Institute at the University of Calgary, Canada. He is also a scientist at the Seaman Family MR Centre, Foothills Medical Centre, Calgary Health Region. In 2003, he was appointed a Canada Research Chair in Image Science. His research focuses in the development and application of new magnetic resonance imaging techniques to the study, detection, and treatment of vascular disease, with specific interests in stroke imaging.

Janet L. Ronsky received the PhD degree in 1994 from the University of Calgary, Canada, in mechanical engineering. She is now a Professor at the Department of Mechanical and Manufacturing Engineering, University of Calgary, Canada. She is also the Director of the Centre for Bioengineering Research and Education and works closely with the Undergraduate Biomedical Engineering Specialization. Professor Ronsky's research group focuses on understanding the links between musculoskeletal system structure, joint mechanics, dynamic joint function, neuromotor control and joint injuries and diseases such as Osteoarthritis. With medical imaging, modeling, and simulation approaches, this knowledge will be applied to develop novel diagnostic and treatment devices and techniques to enhance health care.